IEEE Access
Multidisciplinary ⋮ Rapid Review ⋮ Open Access Journal

Received September 12, 2019, accepted October 19, 2019, date of publication October 23, 2019, date of current version November 6, 2019.

Digital Object Identifier 10.1109/ACCESS.2019.2949181

Automatic Design of a CP Fan-Beam Linear Slotted Array in SIW Technology

SANTI C. PAVONE[1,3], (Member, IEEE), MASSIMILIANO CASALETTI[2], (Member, IEEE), AND MATTEO ALBANI[3], (Fellow, IEEE)

[1]Department of Electrical, Electronics and Information Engineering (DIEEI), University of Catania, 95125 Catania, Italy
[2]Laboratoire d'Électronique et Électromagnétisme (L2E), Sorbonne Université, F-75005 Paris, France
[3]Department of Information Engineering and Mathematics (DIISM), University of Siena, 53100 Siena, Italy

Corresponding author: Santi C. Pavone (santi.pavone@unict.it)

ABSTRACT In this paper, we present a technique for the automatic optimization of a right-hand circular-polarized (RHCP) linear slotted array in substrate integrated waveguide (SIW) technology for the so-called ''last-mile'' communications, in which a narrow (broad) beam is required in the elevation (azimuthal) plane. The procedure can be divided into two steps; *i)* the optimization of isolated single slot pairs, by means of two physics-based functionals able to minimize both slot pair back-scattering and axial-ratio, *ii)* the optimization of the entire linear array of slot pairs, by means of a global functional able to match the co-polar component of the synthesized aperture distribution to the target one, i.e., a uniform magnetic current distribution to radiate a narrow beam in the elevation plane. A prototype of array was optimized at 24.3GHz and measured in the bandwidth [24.1, 24.5]GHz, showing a fair agreement against full-wave simulations, thus validating the exposed techniques.

INDEX TERMS Substrate integrated waveguides (SIW), linear slot array, antennas, sectoral pattern, circular polarization.

I. INTRODUCTION

Substrate integrated waveguides (SIWs) are a promising technology for the design of low-cost and low-profile planar electromagnetic (EM) devices at microwaves/millimeter waves, for the control of guided waves [1]–[5] and for the design of low-cost planar antennas [6]–[10]. They consist of two conveniently spaced rows of metallic pins able to behave as equivalent electric walls. The main advantage of SIWs is undoubtedly their flexibility, i.e. several kinds of passive devices such as filters, power combiners, splitters, cavities, and junctions can be easily designed, and their reduced size, thus allowing scalability at microwaves/millimeter waves. Such kind of devices can be profitably analyzed by adopting *ad hoc* numerical techniques such as the method of moments (MoM) [11], [12] or hybrid methods [13], able to efficiently compute coupling between pins and radiating slots.

On the other hand, in recent years physics-based optimization techniques were successfully developed to design radial-line slot-arrays (RLSA), i.e. radial waveguides loaded by several slots on their top plate, in order to shape an arbitrary desired aperture field distribution, both for antenna [14]–[18] and focusing [19]–[23] applications. In [24], the Authors introduced the technique here investigated to design and optimize a circular polarized (CP) fan-beam linear array in SIW, but neither experimental validation of the proposed technique nor the detailed synthesis of the entire array was presented at that time. Instead, in this paper we extend the automatic techniques developed for the optimization of CP RLSA antennas [15] to design and optimize a sectoral beam CP linear array in SIW technology, by considering not only the slot pair relative positions and lengths are modified during the optimization loop, but also their mutual orientations, in order to improve the polarization purity of the radiated field.

The EM analysis of such structures is performed by using an in-house MoM [11], [12], whereas the optimization loop is based on suitable functionals and geometry-based update rules.

The optimized CP linear slotted array we propose can profitably find application in so-called ''last-mile''

The associate editor coordinating the review of this manuscript and approving it for publication was Wanchen Yang.

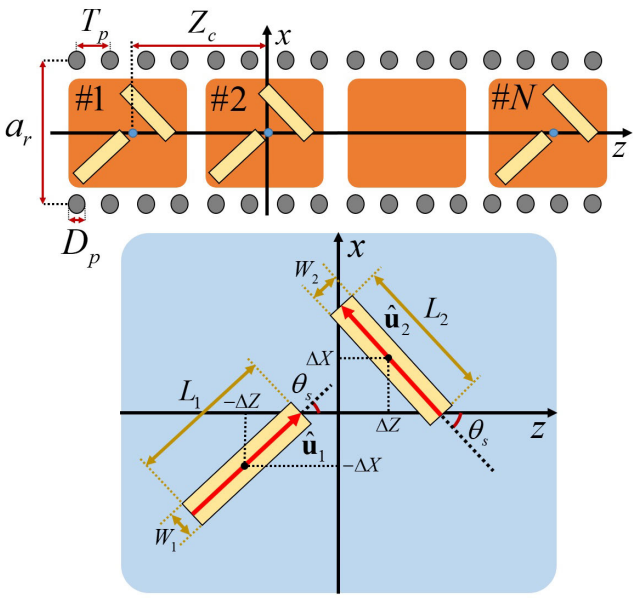

FIGURE 1. Pictorial representation of a RHCP linear array in SIW (top view) and relevant parameters for the definition of physics-based functionals, to be used for single slot pair optimization.

communications (for instance, in rural or sparsely populated areas), in which the antenna is required to radiate a fan beam, i.e., characterized by a broad (narrow) pattern in the azimuthal (elevation) plane.

Section II presents a simple analytical model that allows the definition of two complex functionals and suitable update rules for the geometrical optimization of single right-hand circular polarized (RHCP) slot pair in isolation (i.e., without considering the mutual coupling between adjacent pairs). Such optimized slot pairs are stored in a database (DB) for different lengths and then used as building blocks for synthesizing the starting array configuration. Then, a further optimization loop is developed to take into account also the mutual coupling between different slot pairs, based on a global functional F and associated update rules. To validate the proposed approach, in Section III we present the design of a sectoral pattern RHCP linear array in SIW at 24.3GHz, and a prototype of the array together with measurements. Finally, conclusions are drawn.

II. FORMULATION OF PHYSICS-BASED FUNCTIONALS FOR THE OPTIMIZATION OF CP LINEAR ARRAY IN SIW

In this Section, a simple analytical model is developed in order to define a suitable set of parameters for the optimization of the array unit cell, namely a RHCP pair of slots with centers in $P_{1,2} = (\mp\Delta X, \mp\Delta Z)$ and directed along $\hat{\mathbf{u}}_{1,2} = \pm\sin\theta_s\hat{\mathbf{x}} + \cos\theta_s\hat{\mathbf{z}}$ (Fig. 1). As extensively done in [15], [25], narrow slots can be modeled as equivalent magnetic dipoles, whose moment is $\mathbf{M}_{1,2} = M_{1,2}\hat{\mathbf{u}}_{1,2}$. The SIW is fed by the dominant mode, which can be assumed as a TE^z_{10} mode in an equivalent rectangular waveguide [1]. Its electric and magnetic field distributions can be written as [26]

$$\mathbf{h}^{\mp}_{10} = h^{\mp}_x\hat{\mathbf{x}} + h^{\mp}_z\hat{\mathbf{z}} \text{ and } \mathbf{e}^{\mp}_{10} = e^{\mp}_y\hat{\mathbf{y}}, \text{ with}$$

$$\begin{aligned} h^{\mp}_z &= A\sin\left(\frac{\pi}{a_e}x\right)e^{\mp j\beta_g z}, \\ h^{\mp}_x &= \mp j\frac{\beta_g a_e}{\pi}A\cos\left(\frac{\pi}{a_e}x\right)e^{\mp j\beta_g z}, \\ e^{\mp}_y &= j\omega\mu_0 A\frac{a_e}{\pi}\cos\left(\frac{\pi}{a_e}x\right)e^{\mp j\beta_g z}, \end{aligned} \tag{1}$$

in which the minus (plus) sign applies to waves propagating along the positive (negative) z-direction, β_g is the propagation constant along the waveguide, a_e is the equivalent rectangular waveguide width fitting the fundamental SIW propagating mode, whereas A is an arbitrary modal amplitude.

To optimize slot pair positions and orientations for the linear array design, it is required *i*) to reduce their back-scattering to the feeding point, that is equivalent to minimize the S_{11} parameter, and *ii*) to ensure their RHCP polarization purity, i.e. the magnitude of the axial ratio AR should be also minimized. With reference to Fig. 1, before the optimization, the two slots of the pair are spaced $2\Delta Z = \lambda_g/4$ (being $\lambda_g = 2\pi/\beta_g$ the guided wavelength inside the SIW) to be fed in quadrature and oriented with an angle $\theta_s = \pi/4$ to radiate a circular polarization [15]. Moreover, a fixed displacement along x-direction of $\Delta X = (a_r - D_p)/6$ to avoid slot superposition, and a slot width always linked to its length by the aspect-ratio $W_i = L_i/5$ will be considered throughout the paper.

For the sake of clarity, in Fig. 2 a flowchart of the overall procedure adopted for the linear array optimization is presented, in which also the pertinent sections of the paper associated with each optimization loop are highlighted (orange rectangles).

A. MINIMIZATION OF BACK-SCATTERING BY A SINGLE SLOT PAIR

To minimize slot pair back-scattering, we require the modal amplitude A^-_{10} of the back-reflected wave to vanish. By resorting to the reciprocity theorem [26] and by identifying with $\mathbf{M}_{tot} = M_1\hat{\mathbf{u}}_1 + M_2\hat{\mathbf{u}}_2$ the total magnetic dipole moment of the slot pair, one can easily calculate A^-_{10} as

$$\begin{aligned} A^-_{10} &\propto \iiint_V \mathbf{h}^+_{10}\cdot\mathbf{M}_{tot}dV \\ &= A\left[j\frac{\beta_g a_r}{\pi}\cos\left(\frac{\pi}{a_r}\Delta X\right)\sin\theta_s + \sin\left(\frac{\pi}{a_r}\Delta X\right)\cos\theta_s\right] \\ &\quad\times\left[M_2 e^{-j\beta_g\Delta Z} - M_1 e^{j\beta_g\Delta Z}\right] \to 0. \end{aligned} \tag{2}$$

Since the first term in square brackets cannot be zero, only the second one can be set to zero in order to cancel out single slot pair back-scattering, hence we find that in order to have $|S_{11}| = 0$ it should be $M_1\exp(j\beta_g\Delta Z) = M_2\exp(-j\beta_g\Delta Z)$, or equivalently

$$\begin{aligned} &|M_1| = |M_2|, \\ &\angle M_1 - \angle M_2 = -2\beta_g\Delta Z. \end{aligned} \tag{3}$$

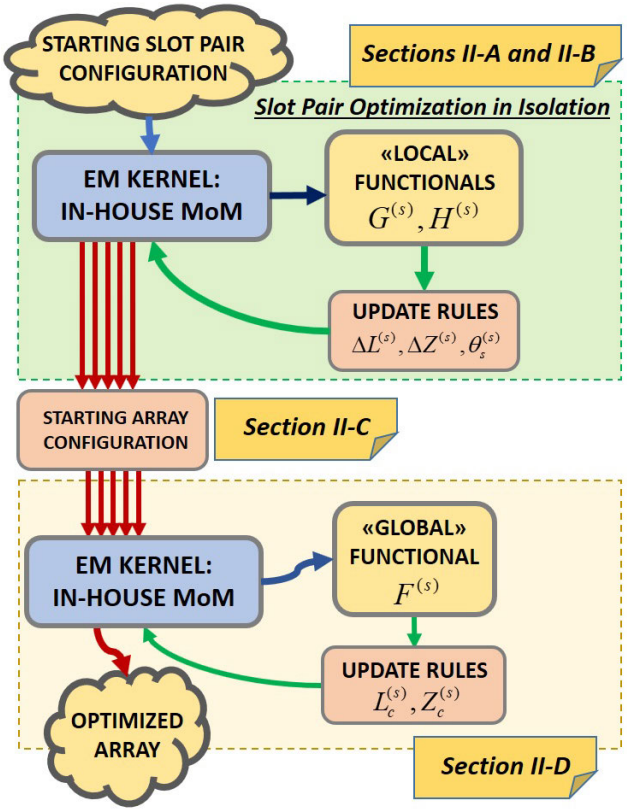

FIGURE 2. Schematic representation of the automatic procedure adopted for the RHCP linear array optimization, in which also the pertinent Sections of the paper are highlighted for simplicity.

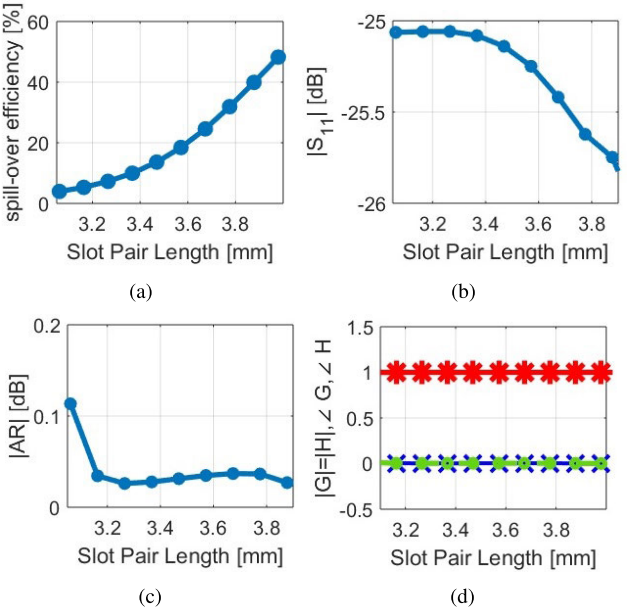

FIGURE 3. Slot pair DB for different slot lengths, after the optimization of single pairs in isolation: (a) slot pair spill-over efficiencies and (b) back-scattering ($|S_{11}|$) in the range of considered lengths; (c) achieved slot pair axial ratio $|AR|$. (d) slot functionals after the optimization loop, namely $|G| = |H| \to 1$ (red asterisks), $\angle H \to 0$ (blue crosses), and $\angle G \to 0$ (green dots). Satisfactory results in terms of polarization purity ($|AR| < 0.2$dB) and back-scattering ($|S_{11}| < -25$dB) are achieved.

Therefore, a complex functional G can be defined in order to minimize the slot pair back-reflection, namely

$$G = \frac{M_1}{M_2} e^{2j\beta_g \Delta Z}, \tag{4}$$

that should be optimized in order to obtain $|G| = 1$, $\angle G = 0$. Since the equivalent magnetic dipole moment M_i of the i-th slot is proportional to its length L_i, for a given average length L_c of the pair one can adjust $|G|$ by setting $L_{1,2} = L_c \mp \Delta L$. The correction ΔL to the slot length is then updated at each iteration step s according to the rule

$$\Delta L^{(s+1)} = \Delta L^{(s)} - \chi_{\Delta L}\left(1 - |G^{(s)}|\right) L_c, \tag{5}$$

in which a suitable damping factor $\chi_{\Delta L} < 1$ was introduced to prevent undesired oscillations of the algorithm. Indeed, (5) is based on the fact that if $|G| > 1$, then $|M_1| > |M_2|$, therefore to adjust $|G| \to 1$, ΔL is increased so that L_1 is reduced and L_2 is increased and in turn, $|M_1|$ decreases and $|M_2|$ increases, so that $|G|$ is finally reduced. Analogous reasoning shows that if $|G| < 1$, ΔL is reduced, accordingly to (4), to increase $|G| \to 1$.

In addition, the displacement between slots can be used to compensate the phase difference between their equivalent magnetic dipole moments $M_{1,2}$, in order to achieve $\angle G = 0$. Hence, according to (4) and by invoking a simple model for slots based on their magnetic polarizability [15], [25], for which $\angle M_{1,2} \approx \pm\beta_g \Delta Z$, then $\angle G \approx \pm 4\beta_g \Delta Z$, the distance between slots of a single pair is updated at each iteration step s according to the rule

$$\Delta Z^{(s+1)} = \Delta Z^{(s)} - \chi_{\Delta z} \frac{\angle G^{(s)}}{4\beta_g}, \tag{6}$$

in which another damping factor $\chi_{\Delta z} < 1$ was introduced.

B. MINIMIZATION OF SINGLE SLOT PAIR AR

In order to have RHCP slot pair such to ensure polarization purity, the cross-polarized LHCP of $\mathbf{M}_{tot}$ has to be set equal to zero, namely

$$\mathbf{M}_{tot} \cdot \hat{\mathbf{p}}_{LH}^{*} \propto M_1 e^{-j\theta_s} + M_2 e^{j\theta_s} \to 0, \tag{7}$$

being θ_s the slot orientation, and $\hat{\mathbf{p}}_{RH,LH} = (\hat{\mathbf{z}} \mp j\hat{\mathbf{x}})/\sqrt{2}$ the RHCP/LHCP polarization unit vectors. Then, by separating the real and imaginary parts in (7), one finds the relations

$$\begin{aligned} &|M_1| = |M_2|, \\ &\angle M_2 - \angle M_1 = \pi - 2\theta_s. \end{aligned} \tag{8}$$

Hence, a proper functional H can be defined to reject the cross-polarized component of the total magnetic dipole moment, i.e.,

$$H = -\frac{M_1}{M_2} e^{-2j\theta_s}. \tag{9}$$

Since by definition $|H| = |G|$, the condition to satisfy $|H| = 1$ is already embedded in (5), then only the condition

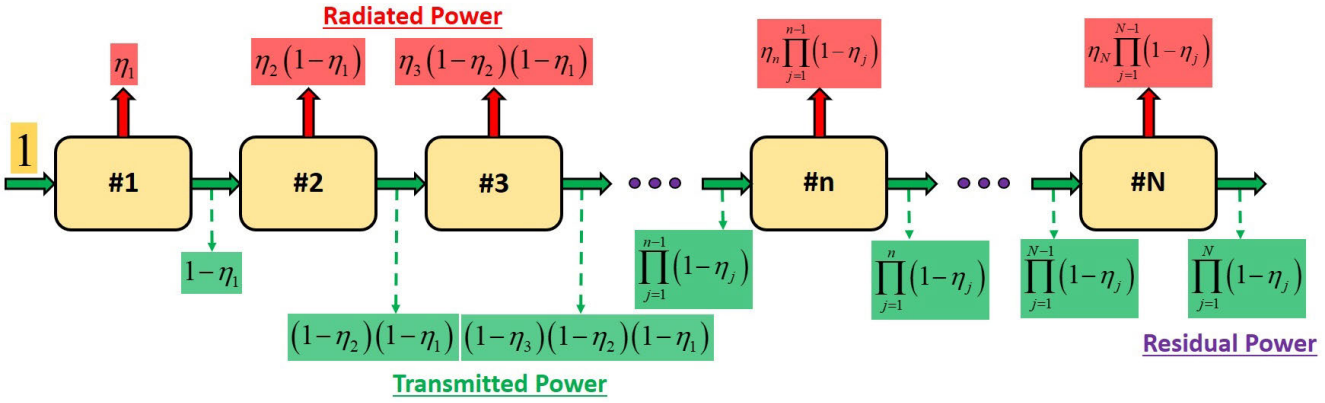

FIGURE 4. Design of the uniform aperture distribution required to radiate a narrow beam in the elevation plane.

$\angle H = 0$ has to be added. It can be realized by defining one more update rule for slot orientations at each iteration step, namely

$$\theta_s^{(s+1)} = \theta_s^{(s)} + \chi_\theta \frac{\angle H^{(s)}}{2}, \tag{10}$$

in which a further damping factor $\chi_\theta < 1$ was introduced to control algorithm convergence.

C. CREATION OF THE OPTIMIZED SLOT PAIR DB

The functionals (4)-(9) and the update rules (5)-(6) and (10) defined in Sects. IIA and IIB can be used to optimize a set of slot pairs for the synthesis of a suitable starting design of the linear array in SIW. Such an approach, although suboptimal because it inherently neglects the mutual coupling between different slot pairs, allows for a faster full optimization (i.e., a smaller number of iterations) of the entire array with respect to that based on an arbitrary choice of the starting aperture distribution.

The set of optimized slot pairs in isolation is parameterized with respect to their lengths in a certain range of interest $L_i \in [L_{min}, L_{max}]$, and then stored in a DB whose entries are the slot geometrical parameters, the achieved axial ratio and the spill-over efficiency, i.e., the ratio of the radiated power by the single slot pair and the incident power on it, as shown in Fig. 3. The spill-over efficiency is of primary importance since it allows the synthesis of the starting aperture distribution to be used for the optimization of the entire linear array, as it will be detailed in the next subsection. The final value of the functionals after the optimization is $G \approx H \approx 1$ for any slot lengths.

D. FULL AUTOMATIC DESIGN OF RHCP LINEAR ARRAY IN SIW

Once developed an automatic technique for single slot pair optimization in terms of back-scattering reduction and polarization purity, a suitable starting design for entire linear array optimization is defined in order to radiate a sectoral pattern in the azimuthal plane, that is a uniform aperture distribution $A = const.$ along the array. In a traveling-wave linear array composed by N slot pairs, a uniform magnitude of the current distribution can be synthesized by properly choosing the spill-over efficiency η_n of each slot pair (i.e., the ratio of radiated power by slot pairs and accepted by the SIW), whereas the constant phase distribution required for radiating a broadside beam is achieved by spacing each slot pair of a uniform amount $Z_c^{(0)} = \lambda_g$ (Fig. 1), being λ_g the wavelength inside the SIW and the superscript (0) is due to the fact that slot pair spacing is imposed only at the beginning of the optimization loop, and then corrected at each iteration step.

With reference to Fig. 4, if a unitary incident power $P_{inc} = 1$W is supposed for simplicity, the spill-over efficiency of each pair should be chosen in such a way to satisfy simultaneously the relations

$$\begin{cases} \eta_1 = \dfrac{1}{N} \\ \eta_2(1-\eta_1) = \dfrac{1}{N} \\ \vdots \quad \vdots \quad \vdots \\ \eta_n \prod_{j=1}^{n-1}(1-\eta_j) = \dfrac{1}{N} \\ \vdots \quad \vdots \quad \vdots \\ \eta_N \prod_{j=1}^{N-1}(1-\eta_j) = \dfrac{1}{N} \end{cases} \tag{11}$$

from which one finds by substitution a general formula for calculating the required efficiency of the i-th slot pair, namely

$$\eta_i = \frac{1}{N-i+1} \qquad \left(i \in [1, N] \cap \mathcal{N}\right). \tag{12}$$

This solution also ensures a vanishing residual power in the waveguide beyond the last slot.

Once the target spill-over efficiency distribution of the array is determined, each slot pair composing the array is synthesized as it was in isolation by resorting to the DB, to find a suitable starting point for the subsequent global optimization. To this aim, a global functional F is then introduced to match the desired magnetic current distribution to

the actual co-polar component of the total magnetic dipole moment as in [15], that is

$$F^{(s)} = \frac{\mathbf{M}^{(s)} \cdot \hat{\mathbf{p}}_{RH}}{A} \frac{\bar{A}}{\bar{M}}, \tag{13}$$

in which the average parameters $\bar{A} = 1/N \sum_{n=1}^{N} |A_n|$ and $\bar{M} = 1/N \sum_{n=1}^{N} |\mathbf{M}_n \cdot \hat{\mathbf{p}}_{RH}|$, being N the number of slot pairs, were used.

Finally, to close the optimization loop, the following rules were developed to update slot pair lengths L_c and positions Z_c, namely

$$\begin{aligned} L_c^{(s+1)} &= L_c^{(s)} \left[1 + \chi_l \left(1 - |F^{(s)}| \sqrt{\eta^{(s)}} \right) \right], \\ Z_c^{(s+1)} &= Z_c^{(s)} + \chi_z \frac{\angle F^{(s)}}{\beta_g}, \end{aligned} \tag{14}$$

in which other two damping factors χ_l, $\chi_z < 1$ were introduced to avoid oscillations of the algorithm.

In the next Section, an example of the automatic design of a linear array in SIW is presented, together with measurements of the realized prototype.

III. PROTOTYPE AND MEASUREMENTS

To prove the effectiveness of the above-described automatic technique, we propose here the design and realization of a sectoral pattern, RHCP SIW linear array, at the central frequency $f = 24.3$GHz. The SIW is realized in a standard ROGERS 6002 substrate of thickness $h_d = 1.524$mm, electrical permittivity $\epsilon_r = 2.94$ and loss tangent $\tan\delta = 0.0012$. According to the design criteria for SIWs described in [1] to prevent higher-order modes to propagate and to minimize leakage effects due to the discretization of continuous electric walls by metallic pins, we found the following geometrical parameters for the SIW: width $a_r = 6.5$mm, pin diameter of $D_p = 0.5$mm, and spacing between adjacent pins of $T_p = 2D_p = 1$mm (Fig. 1).

By calculating the wavenumber dispersion with CST Microwave Studio (Eigenmode Solver), we found the guided wavelength in the SIW structure to be $\lambda_g \approx 8.63$mm at the central frequency. Moreover, we assumed a centrally-fed linear array of length $L = 220$mm composed by $N = 28$ slot pairs, hence the spill-over efficiency distribution of the slot pairs able to synthesize a uniform magnetic current along the linear array was calculated by using (12). A DB of optimized slot pairs with lengths in the range $L_c \in [3, 4]$mm was then created by optimizing each slot pair in isolation according to (4)-(9). In Fig. 3, a summary of the information contained in the DB is presented: indeed in correspondence of each slot pair length belonging to the prescribed range of interest, (a) the pair spill-over efficiency, (b) the slot back-scattering (achieved by minimizing $|S_{11}|$), and the (c) CP polarization purity (achieved by minimizing AR) are optimized, thus obtaining (d) $|G| = |H| \to 1$, $\angle G \to 0$ and also $\angle H \to 0$.

By using the slot pair DB to generate the starting array configuration (Fig. 2), the entire array global optimization was activated to properly take into account the effects of mutual coupling between adjacent slot pairs, according to the functional F in (13) and to the update rules for slot pair lengths L_c and positions Z_c given by (14). In Fig. 5 (a), the complex functional F is shown in magnitude and phase when the optimization process has reached the convergence (35 iterations) and no more significant changes occur in the geometrical parameters if the number of iterations is increased. As it is apparent, the slot pairs in correspondence of the end of the antenna cannot match the requirement $|F| \to 1/\sqrt{\eta}$, due to geometrical unavoidable constraints on their lengths, in order to not overlap the pins of the SIW structure. Moreover, in Fig. 5 (b), the co-polar $|M_{co}|$ and cross-polar

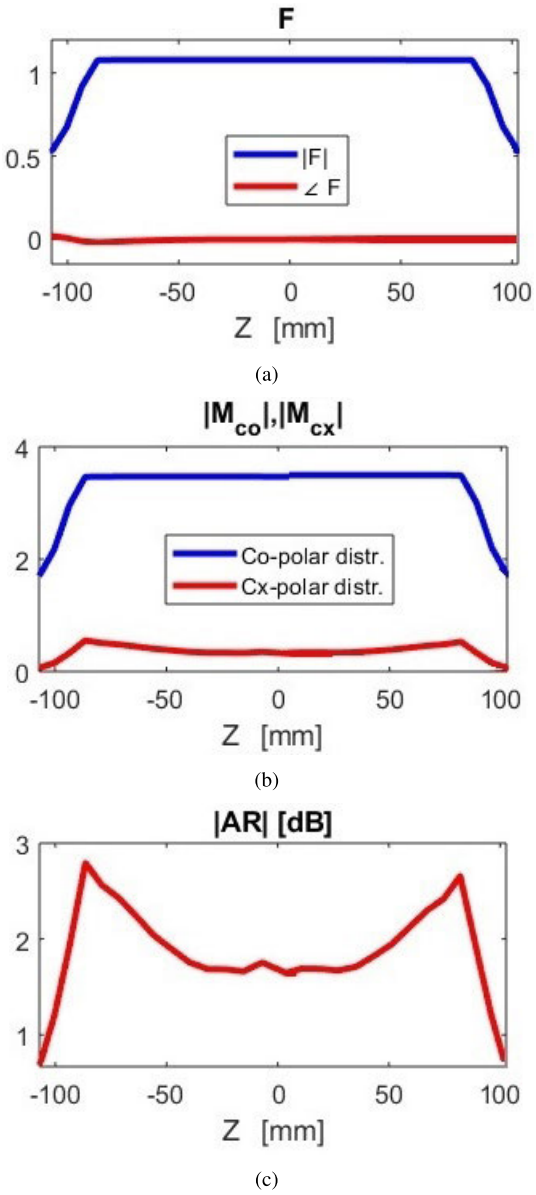

FIGURE 5. Figures of merit after the global optimization loop: (a) achieved F functional (magnitude and phase) after 35 iterations, in correspondence of which the algorithm converges; (b) synthesized co-polar $|M_{co}|$ and cross-polar $|M_{cx}|$ components of the equivalent magnetic current distribution along the linear array; (c) magnitude of the axial ratio $|AR|$ in correspondence of each slot pair.

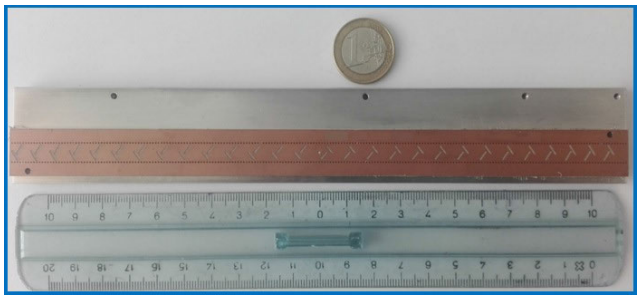

FIGURE 6. Realized prototype of RHCP linear array in SIW at $f = 24.3$GHz.

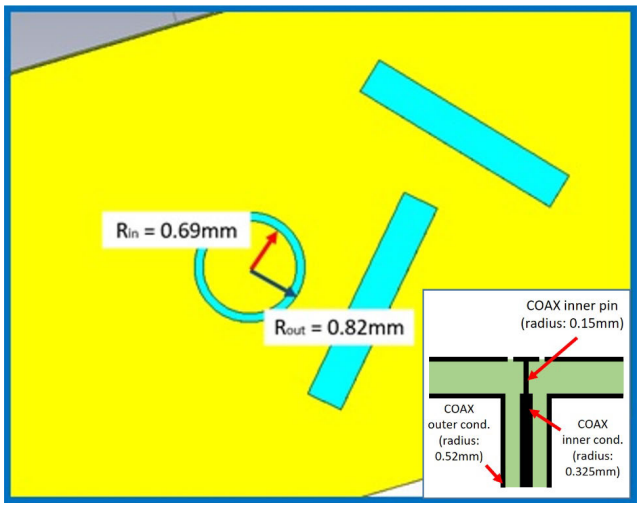

FIGURE 7. Detail of the annular slot used to match the array to the characteristic impedance $Z_0 = 50\Omega$ in the considered bandwidth [24.1, 24.5]GHz. In the inset, geometrical details of the coaxial feed of the antenna.

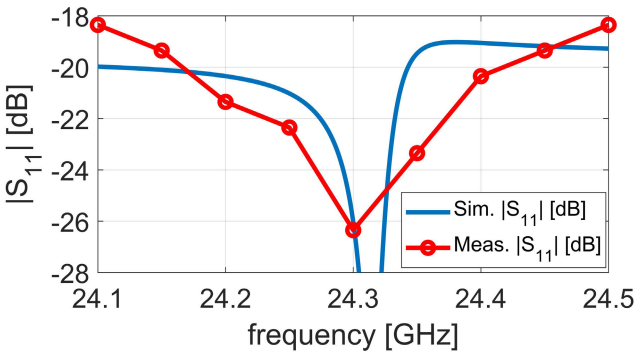

FIGURE 8. Reflection coefficient versus frequency in the considered bandwidth [24.1, 24.5]GHz.

$|M_{cx}|$ magnitudes of the magnetic current distribution synthesized by the linear array are shown, thus demonstrating the efficient rejection of the LH circular polarization. Instead, in Fig. 5 (c), the axial ratio magnitude $|AR|$ is also shown in correspondence of each slot pair.

Finally, a prototype of RHCP linear slotted array in SIW was automatically synthesized at the central frequency and realized by using a standard PCB technology, as shown in Fig. 6. The linear array is fed at its center by the rear pin of a standard SMA flanged panel connector. The coaxial

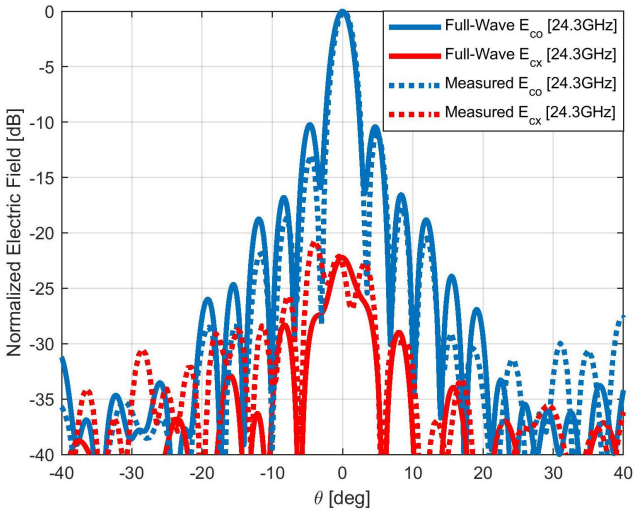

FIGURE 9. Comparison of measured (dotted lines) and simulated (solid lines) normalized co-polar (RHCP) and cross-polar (LHCP) electric field components at the central frequency 24.3GHz (plane at $\phi = 0°$).

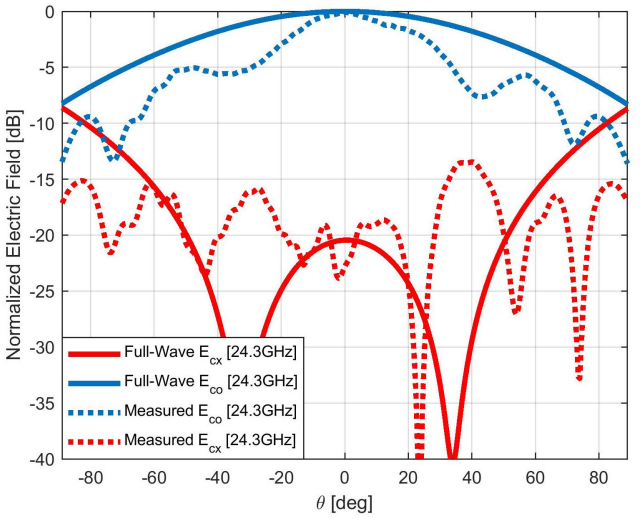

FIGURE 10. Comparison of measured (dotted lines) and simulated (solid lines) normalized co-polar (RHCP) and cross-polar (LHCP) electric field components at the central frequency 24.3GHz (plane at $\phi = 90°$).

feeding has an inner (outer) radius of 0.325mm (0.52mm) and it is filled by a dielectric of permittivity $\epsilon_r = 2.2$. The rear pin of the connector has a smaller radius (0.15mm) than inner conductor of the coaxial feed; it is inserted inside a hole drilled in the dielectric substrate and then soldered to the circular patch on the top copper face of the antenna, as shown in the inset of Fig. 7. An annular slot of inner (outer) radius equal to 0.69mm (0.82mm) is etched on the top metallic plate of the SIW to match the antenna to $Z_0 = 50\Omega$ at the design frequency, as shown in Fig. 7. The simulated and measured reflection coefficients at the coaxial input port are shown versus frequency in Fig. 8, clearly demonstrating the antenna matching.

Measurements of the prototype at central frequency ($f = 24.3$GHz) revealed a nice agreement with the full-wave simulations of the optimized device made by using CST

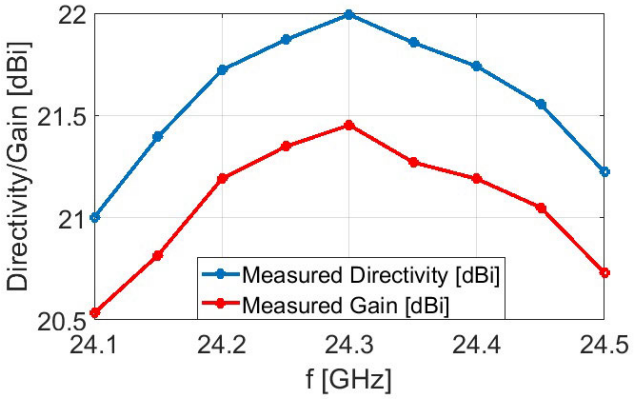

FIGURE 11. Measured maximum directivity and gain versus frequency in the bandwidth [24.1, 24.5]GHz.

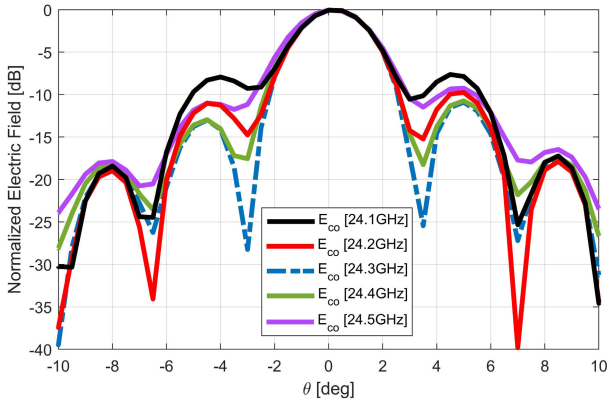

FIGURE 12. Pointing angle stability in the directive plane ($\phi = 0°$) for different frequencies in the considered bandwidth [24.1, 24.5]GHz.

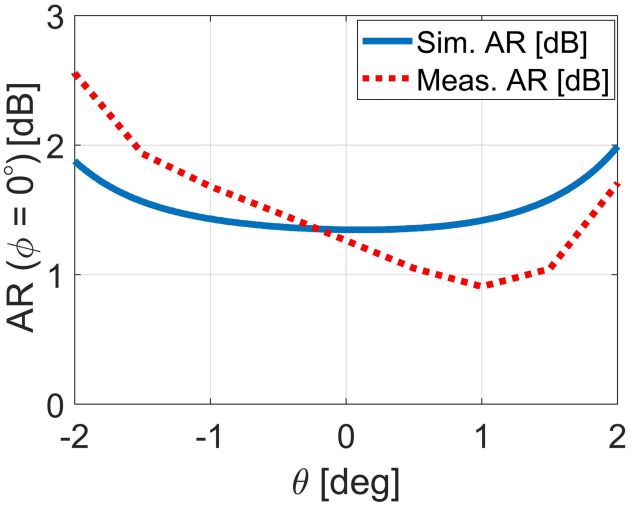

FIGURE 13. Comparison of measured (dotted lines) and simulated (solid lines) axial ratio at the central frequency 24.3GHz (plane at $\phi = 0°$).

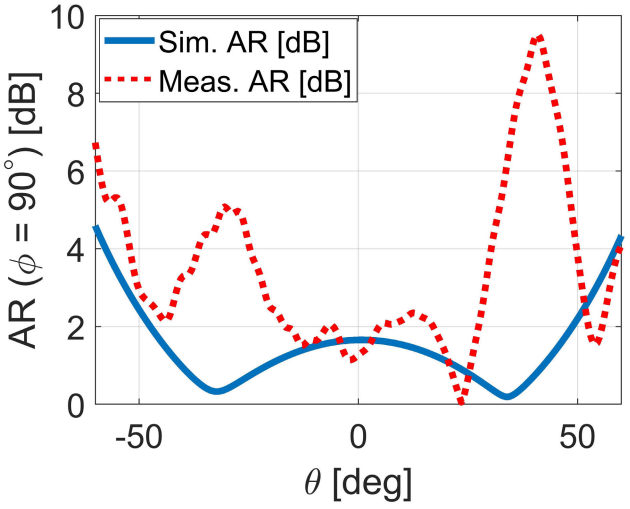

FIGURE 14. Comparison of measured (dotted lines) and simulated (solid lines) axial ratio at the central frequency 24.3GHz (plane at $\phi = 90°$).

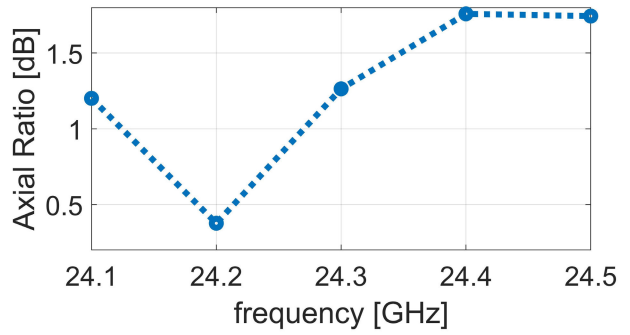

FIGURE 15. Measured axial ratio versus frequency in the considered bandwidth [24.1, 24.5]GHz.

Microwave Studio, as it is apparent from Figs. 9–10: in the plane $\phi = 0°$ ($\phi = 90°$) a narrow (broad) pattern is successfully radiated, as required. Moreover, in Fig. 11 the measured maximum directivity and gain are compared versus frequency in the bandwidth [24.1, 24.5]GHz. At 24.3GHz, we found a directivity (gain) in the direction of maximum radiation $\theta = 0°$ equal to $D_{max} = 22$dBi ($G_{max} = 21.5$dBi), hence the amount of losses due to metal finite conductivity and to the dielectric loss tangent contributes to only 0.5dB. Moreover, in the considered bandwidth [24.1, 24.5]GHz, the antenna gain decreases of approximately 1dB, thus demonstrating also its stability when frequency varies. In Fig. 12, instead, the measured field plot of the antenna directive plane ($\phi = 0°$) is shown at different frequencies in the considered bandwidth, clearly showing a negligible pointing angle tilt versus frequency, but a degradation in terms of side lobe level, as provided by the antenna central feeding.

It is worth noting that in Fig. 10, an oscillation in the measured co-polar (RHCP) component of the radiated field occurs, due to edge effects of the metallic plane on which the antenna is mounted (Fig. 6).

The axial ratio achieved in the direction of maximum radiation $\theta = 0°$ is $|AR| \approx 1.3$dB, thus demonstrating the RHCP polarization purity, as required. For the sake of completeness, in Figs. 13–14 also the comparison between the measured (solid lines) and simulated (dotted lines) axial ratios is provided at the design frequency versus the elevation angle θ, both in the $\phi = 0°$ and $\phi = 90°$ planes. Moreover,

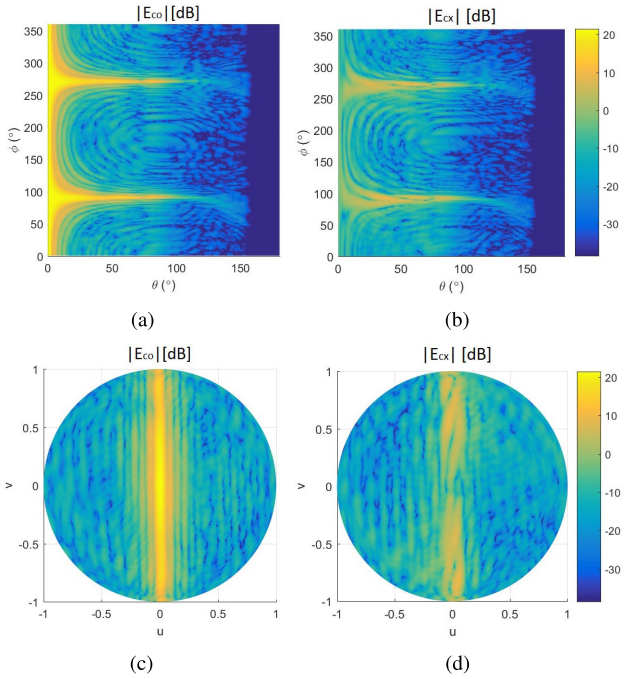

FIGURE 16. Measured electric field maps at the central frequency 24.3GHz: (a) co-polar and (b) cross-polar components in the $\phi - \theta$ plane; (c) co-polar and (d) cross-polar components in the $u - v$ plane.

to demonstrate the antenna polarization purity over the entire bandwidth of interest [24.1, 24.5]GHz, the measured axial ratio versus frequency is shown in Fig. 15.

To conclude, in Fig. 16 the measured maps in the (a)-(b) $\phi - \theta$ and in the (c)-(d) $u - v$ planes of the co-polar (RHCP) and cross-polar (LHCP) components of the radiated electric field are shown at the central frequency.

IV. CONCLUSION

We proposed a fully automatic technique to design a RHCP linear slotted array in SIW technology to radiate a fan-beam. The design technique was based on two subsequent optimization steps: *i)* the first, based on local functionals able to minimize single slot pair back-scattering to the feeding point and its axial ratio, and *ii)* the second based on a global functional that matches the starting aperture distribution to the target uniform one. A prototype of linear array in SIW at $f = 24.3$GHz was successfully optimized, realized and measured in order to validate the overall algorithm.

REFERENCES

[1] D. Deslandes and K. Wu, "Accurate modeling, wave mechanisms, and design considerations of a substrate integrated waveguide," *IEEE Trans. Microw. Theory Techn.*, vol. 54, no. 6, pp. 2516–2526, Jun. 2006.
[2] M. Bozzi, D. Deslandes, P. Arcioni, L. Perregrini, K. Wu, and G. Conciauro, "Efficient analysis and experimental verification of substrate-integrated slab waveguides for wideband microwave applications," *Int. J. RF Microw. Comput.-Aided Eng.*, vol. 15, no. 3, pp. 296–306, May 2005.
[3] M. Bozzi, L. Perregrini, and K. Wu, "Modeling of conductor, dielectric, and radiation losses in substrate integrated waveguide by the boundary integral-resonant mode expansion method," *IEEE Trans. Microw. Theory Techn.*, vol. 56, no. 12, pp. 3153–3161, Dec. 2008.
[4] M. Bozzi, L. Perregrini, and K. Wu, "A novel technique for the direct determination of multimode equivalent circuit models for substrate integrated waveguide discontinuities," *Int. J. RF Microw. Comput.-Aided Eng.*, vol. 19, no. 4, pp. 423–433, 2009.
[5] P. Chu, W. Hong, M. Tuo, and K. Zheng, "Dual-mode substrate integrated waveguide filter with flexible response," *IEEE Trans. Microw. Theory Techn.*, vol. 65, no. 3, pp. 824–830, Mar. 2017.
[6] M. Bozzi, S. A. Winkler, and K. Wu, "Broadband and compact ridge substrate-integrated waveguides," *IET Microw., Antennas Propag.*, vol. 4, no. 11, pp. 1965–1973, 2010.
[7] M. Bozzi, A. Georgiadis, and K. Wu, "Review of substrate-integrated waveguide circuits and antennas," *IET Microw. Antennas Propag.*, vol. 5, no. 8, pp. 909–920, Jun. 2011.
[8] M. Ettorre, R. Sauleau, and L. Le Coq, "Multi-beam multi-layer leaky-wave SIW pillbox antenna for millimeter-wave applications," *IEEE Trans. Antennas Propag.*, vol. 59, no. 4, pp. 1093–1100, Apr. 2011.
[9] K. Tekkouk, M. Ettorre, L. Le Coq, and R. Sauleau, "SIW pillbox antenna for monopulse radar applications," *IEEE Trans. Antennas Propag.*, vol. 63, no. 9, pp. 3918–3927, Sep. 2015.
[10] Y. Lyu, X. Liu, D. Erni, and Q. Wu, "Leaky-wave antennas based on noncutoff substrate integrated waveguide supporting beam scanning from backward to forward," *IEEE Trans. Antennas Propag.*, vol. 64, no. 6, pp. 2155–2164, Jun. 2016.
[11] M. Casaletti, R. Sauleau, M. Ettorre, and S. Maci, "Efficient analysis of metallic and dielectric posts in parallel-plate waveguide structures," *IEEE Trans. Microw. Theory Techn.*, vol. 60, no. 10, pp. 2979–2989, Oct. 2012.
[12] M. Casaletti, G. Valerio, R. Sauleau, and M. Albani, "Mode-matching analysis of lossy SIW devices," *IEEE Trans. Microw. Theory Techn.*, vol. 64, no. 12, pp. 4126–4137, Dec. 2016.
[13] D. Dahl, H.-D. Brüns, L. Wang, E. Frick, C. Seifert, M. Lindner, and C. Schuster, "Efficient simulation of substrate-integrated waveguide antennas using a hybrid boundary element method," *IEEE J. Multiscale Multiphys. Comput. Tech.*, vol. 4, pp. 180–189, 2019.
[14] M. Albani, G. L. Cono, R. Gardelli, and A. Freni, "An efficient full-wave method of moments analysis for RLSA antennas," *IEEE Trans. Antennas Propag.*, vol. 54, no. 8, pp. 2326–2336, Aug. 2006.
[15] M. Albani, A. Mazzinghi, and A. Freni, "Automatic design of CP-RLSA antennas," *IEEE Trans. Antennas Propag.*, vol. 60, no. 12, pp. 5538–5547, Dec. 2012.
[16] G. Montisci, M. Musa, and G. Mazzarella, "Waveguide slot antennas for circularly polarized radiated field," *IEEE Trans. Antennas Propag.*, vol. 52, no. 2, pp. 619–623, Feb. 2004.
[17] G. Montisci, "Design of circularly polarized waveguide slot linear arrays," *IEEE Trans. Antennas Propag.*, vol. 54, no. 10, pp. 3025–3029, Oct. 2006.
[18] A. Tamayo-Dominguez, J.-M. Fernandez-Gonzalez, and M. S. Castaner, "Low-cost millimeter-wave antenna with simultaneous sum and difference patterns for 5G point-to-point communications," *IEEE Commun. Mag.*, vol. 56, no. 7, pp. 28–34, Jul. 2018.
[19] A. Mazzinghi, M. Balma, D. Devona, G. Guarnieri, G. Mauriello, M. Albani, and A. Freni, "Large depth of field pseudo-Bessel beam generation with a RLSA antenna," *IEEE Trans. Antennas Propag.*, vol. 62, no. 8, pp. 3911–3919, Aug. 2014.
[20] M. Albani, S. C. Pavone, M. Casaletti, and M. Ettorre, "Generation of non-diffractive Bessel beams by inward cylindrical traveling wave aperture distributions," *Opt. Express*, vol. 22, pp. 18354–18364, 2014.
[21] S. C. Pavone, M. Ettorre, M. Casaletti, and M. Albani, "Transverse circular-polarized Bessel beam generation by inward cylindrical aperture distribution," *Opt. Express*, vol. 24, no. 10, pp. 11103–11111, 2016.
[22] S. C. Pavone, M. Ettorre, and M. Albani, "Analysis and design of Bessel beam launchers: Longitudinal polarization," *IEEE Trans. Antennas Propag.*, vol. 22, no. 6, pp. 2311–2318, Jun. 2016.
[23] S. C. Pavone, A. Mazzinghi, A. Freni, and M. Albani, "Comparison between broadband Bessel beam launchers based on either Bessel or Hankel aperture distribution for millimeter wave short pulse generation," *Opt. Express*, vol. 25, no. 16, pp. 19548–19560, 2017.
[24] S. C. Pavone, M. Casaletti, and M. Albani, "Automatic design of a RHCP linear slot array in substrate integrated waveguide," in *Proc. 12th Eur. Conf. Antennas Propag. (EuCAP)*, 2018, pp. 1–3.
[25] H. A. Bethe, "Theory of diffraction by small holes," *Phys. Rev. Lett.*, vol. 66, nos. 7–8, pp. 163–182, Oct. 1944.
[26] C. A. Balanis, *Advanced Engineering Electromagnetics*. Hoboken, NJ, USA: Wiley, 2012.

SANTI C. PAVONE was born in Patti (ME), Italy, in 1988. He received the B.Sc. *(summa cum laude)* and M.Sc. *(summa cum laude)* degrees in electronics engineering from the University of Messina, Messina, Italy, in 2010 and 2012, respectively, and the Ph.D. degree (with the additional label of Doctor Europaeus) in information engineering and science (electromagnetics engineering) from the University of Siena, Siena, Italy, in 2015.

He was a Visiting Ph.D. Student with the Institut d'Électronique et de Télécommunications de Rennes (IETR), Université de Rennes 1, Rennes, France, for five months, in 2015. From 2016 to 2019, he was an Associate Researcher with the Laboratory of Applied Electromagnetics, University of Siena. Since 2019, he has been an Assistant Professor with the Department of Electrical, Electronics, and Information Engineering (DIEEI), University of Catania, Italy. His current research interests include fundamental electromagnetic theory, RADAR design at millimeter waves, high-frequency techniques, focusing systems, non-diffractive localized pulses, and leaky-wave reconfigurable antennas based on liquid crystals.

Dr. Pavone was a recipient of the ESF Research Networking Programme NEWFOCUS Scholarship, in 2015, and the IEEE Antennas and Propagation Society Student Award, Chapter Central-Southern Italy, in 2014. In 2017, he was a Finalist of the Best Paper Award in electromagnetics and antenna theory at the 11th European Conference on Antennas and Propagation, Paris. In 2018, he was a co-recipient of the Best Paper Award in electromagnetics and antenna theory at the 12th European Conference on Antennas and Propagation, London, U.K. In 2019, he was a recipient of the Young Scientist Award (YSA) from the 41st Progress in Electromagnetics Research Symposium (PIERS 2019), Rome, Italy. He serves as an Associate Editor of IEEE Access.

MASSIMILIANO CASALETTI was born in Siena, Italy, in 1975. He received the Laurea degree in telecommunications engineering and the Ph.D. degree in information engineering from the University of Siena, Siena, Italy, in 2003 and 2007, respectively.

From 2003 to 2005, he was with the Research Center MOTHESIM, Les Plessis Robinson, Paris, France, under EU Grant RTN-AMPER (RTN: Research Training Network and AMPER: Application of Multiparameter Polarimetry). He has been a Research Associate with the University of Siena from 2006 to 2010, and a Postdoctoral Researcher with the Institut d'Electronique et des Télécommunications de Rennes (IETR), University of Rennes 1, Rennes, France, from 2010 to 2013. He is currently an Associate Professor with the Sorbonne Université, Paris, France. His current research interests include numerical methods for electromagnetic (scattering, antennas, and microwave circuits), metasurface structures, field beam expansion methods, and electromagnetic band-gap structures.

Dr. Casaletti was a co-recipient of the Best Poster Paper Award at the Third European Conference on Antennas and Propagation (EuCAP-2009), Berlin, Germany, and a recipient of the Honorable Mention for Antenna Theory at EuCAP-2010, Barcelona, Spain, and the Best Paper Award on Antenna Theory at EuCAP-2011, Rome, Italy.

MATTEO ALBANI received the Laurea degree in electronic engineering and the Ph.D. degree in telecommunications engineering from the University of Florence, Florence, Italy, in 1994 and 1999, respectively.

He is currently an Associate Professor with the Information Engineering and Mathematics Department, University of Siena, Siena, Italy, where he is also the Director of the Applied Electromagnetics Laboratory. From 2001 to 2005, he was an Assistant Professor with the University of Messina, Messina, Italy. He coauthored more than 80 journal articles and book chapters, more than 200 conference articles, and five patents. His current research interests include high-frequency methods for electromagnetic scattering and propagation, numerical methods for array antennas, antenna analysis and design, and metamaterials and metasurfaces.

Dr. Albani is a member of EurAAP and URSI. He received the G. Barzilai Young Researcher Best Paper Award from the XIV RiNEM, Ancona, Italy, in 2002, and the URSI Commission B Young Scientist Award from URSI EMTS, Pisa, Italy, in 2004. He was a Coauthor and Advisor of the winners of the Best Paper Award at the First European AMTA Symposium 2006, Munich, Germany, and the third Prize Young Scientist Best Paper Award from 2010 URSI EMTS, Berlin, Germany. With his Coauthor, he received the Antenna Theory Best Paper Award from the EuCAP 2014, den Haag, The Netherlands, and the Antenna Theory Best Paper Award from the EuCAP 2018, London, U.K.